Polarization of hypernuclei in the (π^+, K^+) reaction

H. Bandō

Division of Mathematical Physics, Fukui University, Fukui 910, Japan

T. Motoba

Laboratory of Physics, Osaka Electro-Communication University, Neyagawa, Osaka 572, Japan

M. Sotona and J. Žofka*

Nuclear Physics Institute, Czechoslovak Academy of Sciences, 25068 Řež, Czechoslovakia

(Received 11 October 1988)

Cross sections and polarizations for the (π^+, K^+) hypernuclear production reaction are newly formulated in the correct full scheme based on both the elementary spin-nonflip f and the spin-flip g amplitudes, avoiding thus previous approximations and oversimplifications. Importance of this novel formulation is demonstrated for ^{12}C, ^{16}O, ^{28}Si, and ^{56}Fe targets. Particular states indeed acquire both large cross sections and large polarizations, which has an important bearing on experimental projects.

I. INTRODUCTION

The (π^+, K^+) reaction has proved to be a powerful and selective method to produce hypernuclear states with a surface nucleon hole and a Λ hyperon in a series of orbits [including even the deepest $(0s)_\Lambda$] in light-to-heavy hypernuclei.[1-5] The characteristics of the (π^+, K^+) reaction are, in this regard, complementary to the in-flight (K^-, π^-) reaction[6] which preferentially excites substitutional states.

The (π^+, K^+) reaction has been so far applied to singles experiments only, while the (K^-, π^-) reaction was used for coincidence experiments by measuring the decay particles (γ or weak-decay π^-, p and n).[7,8] When applied to coincidence experiments, a remarkable advantage of the (π^+, K^+) process would be its ability to yield large polarization in the produced hypernucleus, which is, in turn, very useful in the successive coincidence experiment.[9] The elementary process $\pi^- p \rightarrow K^0 \Lambda$ (and, therefore, $\pi^+ n \rightarrow K^+ \Lambda$ also) is experimentally known to give a large positive polarization for Λ hyperon at $p_\pi \sim 1$ GeV/c (Ref. 10) which is in the optimal momentum range for Λ-hypernuclear production.

The hypernuclear polarization was studied theoretically for the first time in Refs. 11 and 12, but the actual calculation there was limited to polarization of the orbital angular momenta, which arises from the absorptions of the incoming and outgoing mesons in the medium without any spin-flip interaction introduced. Recently the elementary $\pi^- p \rightarrow K^0 \Lambda$ data were reanalyzed[13] on the basis of the previous works,[10] so that the spin-nonflip f and spin-flip g amplitudes became available even in a convenient form of tabulated numbers. As expected from the large elementary polarization, the g amplitudes are significantly large.

The aim of this paper is first to reformulate the polarization of hypernucleus produced in the (π^+, K^+) reaction in terms of all elementary amplitudes (without neglecting spin-flip terms g, which leads to nontrivial interference effects in both cross section and polarization), distorted meson waves and nuclear (hypernuclear) wave functions. Secondly, the polarizations are calculated for some interesting targets (^{12}C, ^{16}O, ^{28}Si, ^{56}Fe) and final hypernuclear states. An attractive feature is the kinematical constraint on the hypernuclear polarization due to the particular quantum numbers carried by the initial and final states. Equally interesting is the interplay between the two sources of the polarization, namely, the f-g interference and the meson absorptions in the medium.

In this exploratory study, we adopt a simple (but reasonably working) model of Λ-particle N-hole configurations, distortions are treated in the eikonal approximation, no Fermi motion averaging is attempted and the continuum influence is neglected here. These simplifications are commonly adopted and should not mask or significantly change the effects, demonstration of which is aimed at here. Also, the distinction should be kept in mind between definitions of the Λ-hyperon polarization in the elementary process and in the many-body hypernuclear one. In the latter, the Λ-hyperon polarization (changed as compared to the elementary process) is superimposed on that of the nuclear core and a genuine hypernuclear effect results.

Section II is devoted to the presentation of general expressions for the cross section and polarization. In Sec. III, the calculated results are shown and discussed. Concluding remarks are given in Sec. IV.

II. CROSS SECTIONS AND POLARIZATION

We consider a (π^+, K^+) reaction on a nuclear target,

$$\pi^+ + {}^A Z(J_i) \rightarrow K^+ + {}_\Lambda^A Z(J_f) ,$$

with J_i and J_f denoting the spins of the target nucleus and the final hypernucleus, respectively. The differential

cross section in the laboratory (lab.) frame is expressed as

$$\frac{d\sigma}{d\Omega_{\text{lab}}}(\theta_{\text{lab}}) = \gamma \frac{(2\pi)^4 p_K^2 E_\pi E_K E_H}{p_\pi [p_K(E_H + E_K) - p_\pi E_K \cos\theta_{\text{lab}}]} \overline{|T_{if}^{\text{lab}}|^2} ,$$

(1)

$$\gamma = \tfrac{2}{3} \cdot 389.4 \ [\mu b/sr \cdot (GeV/c)^2] ,$$

(2)

where θ_{lab} is the laboratory angle for the K^+ meson, and p's and E's are momenta and energies in the A-body (nuclear target) laboratory frame, respectively. (E_H is that for the hypernucleus $_\Lambda^A Z$.) The factor γ should be there when the unit GeV/c is used for momenta and the amplitudes given in Ref. 13 are employed. The squared lab. T-matrix element averaged over angular momentum projections, $\overline{|T_{if}^{\text{lab}}|^2}$, is given in the "frozen-nucleon" approximation by

$$\overline{|T_{if}^{\text{lab}}|^2} = \sum_{M_f} R(if;M_f) ,$$

(3)

$$R(if;M_f) = \frac{1}{[J_i]} \sum_{M_i} \left| \langle J_f M_f | \int d^3 r \chi^{(-)}(\mathbf{p}_K;\mathbf{r})^* \chi^{(+)}(\mathbf{p}_\pi;\mathbf{r}) \sum_{k=1}^{A} U_-(k)\delta(\mathbf{r}-\mathbf{r}_k) \cdot \lambda[f + ig(\boldsymbol{\sigma}_k \hat{\mathbf{n}})] | J_i M_i \rangle \right|^2 ,$$

(4)

where χ denotes the meson distorted wave and U_- is an operator converting a neutron into a Λ hyperon. An abbreviation $[J] \equiv 2J + 1$ is used throughout. The factor λ accounts for the lab.-c.m. transformation in the two-body (nucleon-target) frame and is given by

$$\lambda = \frac{1}{16\pi^2} \left[\frac{(E_\Lambda + m_\Lambda)(E_N + m_N)}{(\epsilon_\Lambda + m_\Lambda)(\epsilon_N + m_N)} \right]^{1/2} \left[\frac{1}{E_K E_\Lambda E_\pi E_N} \right]^{1/2} \left[2(\epsilon_\pi + \epsilon_N) + (m_\Lambda + m_N) + E_K + E_\pi + \frac{p_K^2 - p_\pi^2}{E_\Lambda + m_\Lambda} \right] ,$$

(5)

where ϵ's are the energies in the two-body c.m. frame, and p's and E's represent, differently from those explicit in Eqs. (3) and (4), the momenta and energies in the two-body lab. frame. The c.m. amplitudes f (spin-nonflip) and g (spin-flip) are functions of the incident π^+ momentum and the angle of the outgoing K^+, and are given in Ref. 13 in numerical form. $\hat{\mathbf{n}}$ is a unit vector perpendicular to the reaction plane. Very small kinematical mixing of f and g amplitudes, when going to the A-body frame, is discussed elsewhere and it is neglected here.

In the following we use two different orthogonal frames called S_1 and S_2:

$$\{S_1\}: \ \hat{\mathbf{z}}_1 = \hat{\mathbf{q}}, \ \hat{\mathbf{y}}_1 = [\mathbf{p}_\pi \times \mathbf{p}_K]/|\mathbf{p}_\pi \times \mathbf{p}_K| = \hat{\mathbf{n}} ,$$

$$\hat{\mathbf{x}}_1 = \hat{\mathbf{y}}_1 \times \hat{\mathbf{z}}_1 \ (\mathbf{q} = \mathbf{p}_\pi - \mathbf{p}_K) ,$$

(6)

$$\{S_2\}: \ \hat{\mathbf{z}}_2 = \hat{\mathbf{n}}, \ \hat{\mathbf{y}}_2 = \hat{\mathbf{q}}, \ \hat{\mathbf{x}}_2 = \hat{\mathbf{y}}_2 \times \hat{\mathbf{z}}_2 .$$

(7)

Here we define the magnetic subspace population $P(if;M_f)$ in the S_2 frame by using $R(if;M_f)$ of Eq. (4) as

$$P(if;M_f) = \frac{R(if;M_f)}{\sum_{M_f} R(if;M_f)} \ \text{in} \ \{S_2\} ,$$

(8)

where M_f is quantized perpendicularly to the reaction plane. Physical meaning of $P(if;M_f)$ is lucid. In terms of this magnetic subspace population $P(if;M_f)$, the polarization of the hypernuclear state $|J_f\rangle$ is defined as

$$\mathcal{P}(if) = \sum_{M_f} M_f P(if;M_f)/J_f .$$

(9)

The polarization measures the extent of population asymmetry with respect to the reaction plane. Note that the θ_{lab} dependences are implicit in $P(if;M_f)$ and $\mathcal{P}(if)$.

The product of the meson distorted waves is expanded in partial waves:

$$\chi^{(-)}(\mathbf{p}_K;\mathbf{r})^* \chi^{(+)}(\mathbf{p}_\pi;\mathbf{r})$$

$$= \sum_{km} \sqrt{4\pi[k]} i^k \tilde{j}_{km}(p_\pi, p_K, \theta; r) Y_{km}(\hat{\mathbf{r}}) .$$

(10)

In the limit of plane waves, $\chi^* \chi$ tends to e^{iqr} and $\tilde{j}_{km}$ to $j_k(qr)\delta_{m0}$ in the S_1 frame. Since evaluation of $\tilde{j}_{km}$ is easier in the S_1 frame, we make transformation from $\{S_2\}$ to $\{S_1\}$ in the course of kinematical reduction of Eq. (4). The transformation is

$$\langle J_f || \tilde{j}_{km} Y_k || J_i \rangle_{S_2}$$

$$= \sum_{m'} D_{m'm}^k(\Omega_{12})^* \langle J_f || \tilde{j}_{km'} Y_k || J_i \rangle_{S_1} ,$$

(11)

$$\Omega_{12} = \left[\frac{\pi}{2}, \frac{\pi}{2}, \frac{\pi}{2} \right] .$$

(12)

Equation (4) for $R(if, M_f)$ consists of three terms:

$$R(if, M_f) = \lambda^2 \{ |f|^2 \rho^{ff}(if;M_f) + |g|^2 \rho^{gg}(if;M_f)$$

$$+ 2 \text{Im}[fg^* \rho^{fg}(if;M_f)] \} .$$

(13)

The explicit expressions of these three "reduced effective numbers" $\rho(if;M_f)$ are given in the Appendix. Correspondingly, $\overline{|T_{if}^{\text{lab}}|^2}$ of Eq. (3) is also expressed as a sum of

three contributions:

$$\overline{|T_{if}^{\text{lab}}|^2} = \lambda^2 \{ |f|^2 N^{ff}(if) + |g|^2 N^{gg}(if) + 2\,\text{Im}[fg^* N^{fg}(if)] \} , \tag{14}$$

$$N(if) = \sum_{M_f} \rho(if; M_f) . \tag{15}$$

The N's here are generalizations of the "effective neutron

number" which has been used often.

In a special case where the target nucleus has spin zero $(J_i = 0)$ and the produced hypernuclear state is characterized by a particle-hole configuration

$$[N^{-1}\Lambda]_J \equiv [(n_N l_N j_N)^{-1}(n_\Lambda l_\Lambda j_\Lambda)]_J ,$$

the expressions of $\rho(if; M_f)$ are further reduced:

$$\rho^{ff}([N^{-1}\Lambda]_J; M) = [j_\Lambda][j_N](j_\Lambda \tfrac{1}{2} j_N - \tfrac{1}{2}|J0)^2 \sum_K (-)^M (JMJ - M|K0) B_K^{ff} \quad (l_\Lambda + l_N + J = \text{even}) , \tag{16}$$

$$B_K^{ff} = \sum_{m_1 m_2} (-)^{m_2}(Jm_1 J - m_2|Kq)i^{|q|}d(K,q)\mathscr{A}(Jm_1)\mathscr{A}(Jm_2)^* , \tag{17}$$

$$\rho^{gg}([N^{-1}\Lambda]_J; M) = -6[l_\Lambda][l_N][j_\Lambda][j_N][J]\sum_K (-)^M (JMJ - M|K0) B_K^{gg} , \tag{18}$$

$$B_K^{gg} = \sum_m (-)^K (J - mJm|K0) \sum_{k_1 k_2} \sum_{pp'} (JmJ - m|p0)(k_1 - mk_2m|p0)$$

$$\times (k_1 m k_2 - m|p'0)W(JJk_1k_2; p1) \begin{Bmatrix} l_\Lambda & \tfrac{1}{2} & j_\Lambda \\ l_N & \tfrac{1}{2} & j_N \\ k_1 & 1 & J \end{Bmatrix} \begin{Bmatrix} l_\Lambda & \tfrac{1}{2} & j_\Lambda \\ l_N & \tfrac{1}{2} & j_N \\ k_2 & 1 & J \end{Bmatrix}$$

$$\times \sqrt{[k_1][k_2]}(-)^{k_1 + k_2} i^{k_1 - k_2}(l_N 0 l_\Lambda 0|k_1 0)(l_N 0 l_\Lambda 0|k_2 0)$$

$$\times \sum_{m_1 m_2} (-)^{m_2}(k_1 m_1 k_2 - m_2|p'q)i^{|q|}d(p',q)\mathscr{A}(k_1 m_1)\mathscr{A}(k_2 m_2)^* , \tag{19}$$

$$\rho^{fg}([N^{-1}\Lambda]_J; M) = \sqrt{6[l_\Lambda][l_N]}[j_\Lambda][j_N][J](-)^{l_\Lambda + (1/2) - j_\Lambda}(j_\Lambda \tfrac{1}{2} j_N - \tfrac{1}{2}|J0)$$

$$\times (l_N 0 l_\Lambda 0|J0) \begin{Bmatrix} l_\Lambda & \tfrac{1}{2} & j_\Lambda \\ l_N & \tfrac{1}{2} & j_N \\ J & 1 & J \end{Bmatrix} \sum_K (-)^M (JMJ - M|K0) B_K^{fg} , \tag{20}$$

$$B_K^{fg} = \sum_p (-)^{K+p}\sqrt{[p]}(p010|K0)W(JJK1; pJ) \sum_{m_1 m_2} (-)^{m_2}(Jm_1 J - m_2|pq)i^{|q|}d(p,q)\mathscr{A}(Jm_1)\mathscr{A}(Jm_2)^* , \tag{21}$$

where $\mathscr{A}(km)$ is the radial matrix element defined by

$$\mathscr{A}(km) = \langle \phi_{n_\Lambda l_\Lambda j_\Lambda}(r) || \tilde{j}_{km}(p_\pi, p_K, \theta; r) || \phi_{n_N l_N j_N}(r) \rangle_{S_1} , \tag{22}$$

$$\mathscr{A}(k - m) = (-)^m \mathscr{A}(km) . \tag{23}$$

As can be seen in Eqs. (16), (18), and (20), $B_{K=\text{even}}$ contribute to the effective neutron number Eq. (15) (hence, to the cross section) but not to the polarization Eq. (9), while $B_{K=\text{odd}}$ only to the polarization.

III. RESULTS AND DISCUSSION

It may be instructive to consider first the no-distortion [plane-wave (PW)] limit where $\mathscr{A}(km) = \mathscr{A}(k0)\delta_{m0}$. Then it is readily seen in Eqs. (17), (19), and (21) that $B_{K=\text{odd}}^{ff}$, $B_{K=\text{odd}}^{gg}$ and $B_{K=\text{even}}^{fg}$ vanish. This is as expected because without meson-distortion-originated polarization only fg^* combination contributes to the polarization. In this connection, the polarization in the elementary $\pi^+ n \rightarrow \Lambda K^+$ reaction is given by

$$\mathscr{P}_\Lambda^{\text{elem}} = \frac{2\,\text{Im}[fg^*]}{|f|^2 + |g|^2} . \tag{24}$$

For some typical $[N^{-1}\Lambda]_J$ states we obtain

$$\mathscr{P}^{\text{PW}}([p_{3/2N}^{-1}s_{1/2\Lambda}]_{J=1^-}) = \frac{-4\,\text{Im}[fg^*]}{4|f|^2 + |g|^2} , \tag{25}$$

$$\mathscr{P}^{\text{PW}}([p_{1/2N}^{-1}s_{1/2\Lambda}]_{J=1^-}) = \frac{2\,\text{Im}[fg^*]}{|f|^2 + |g|^2} , \tag{26}$$

$$\mathscr{P}^{\text{PW}}([p_{3/2N}^{-1}p_{1/2\Lambda}]_{J=2^+}) = \frac{-6\,\text{Im}[fg^*]}{4|f|^2 + 3|g|^2} , \tag{27}$$

$$\mathscr{P}^{\text{PW}}([p_{1/2N}^{-1}p_{3/2\Lambda}]_{J=2^+}) = \frac{6\,\text{Im}[fg^*]}{4|f|^2 + 3|g|^2} . \tag{28}$$

It is noticed that $\mathcal{P}^{\mathrm{PW}}=0$ holds for all substitutional $[(lj)^{-1}(lj)]_J$ configurations and for all unnatural parity states (namely, for all other than the above four). Note also that $\mathcal{P}^{\mathrm{PW}}$ is independent of the nuclear matrix element $\mathcal{A}$ of Eq. (22) and only depends on the f and g amplitudes in the manner pertinent to the kinematical specification of the state.

In Table I, we illustrate the angular dependence of the polarization $\mathcal{P}^{\mathrm{PW}}$ in the (π^+,K^+) reaction at $p_\pi=1.04$ GeV/c. Reflecting the large $\mathcal{P}_\Lambda^{\mathrm{elem}}$ values in the elementary process, the polarizations in the four states shown exceed 50% already at $\theta_{\mathrm{lab}}=15°-20°$.

To see explicitly the interplay of the two different origins of polarization (spin versus orbital angular momentum, or, f-g interference versus meson absorption), we give algebraic expressions for the polarizations

$$\mathcal{P}([p_{3/2N}^{-1}s_{1/2\Lambda}]_{J=1^-})$$

and

$$\mathcal{P}([p_{1/2N}^{-1}s_{1/2\Lambda}]_{J=1^-}) \, ,$$

which are pertinent to the ground states of $^{12}_\Lambda$C and $^{16}_\Lambda$O, respectively, produced in the (π^+,K^+) reaction

$$\mathcal{P}([p_{jN}^{-1}s_{1/2\Lambda}]_{J=1^-})=\frac{\mathcal{P}^{\mathrm{PW}}+\mathcal{P}^A}{1+\mathcal{P}^{\mathrm{PW}}\mathcal{P}^A} \, , \quad (29)$$

where $\mathcal{P}^{\mathrm{PW}}$ are given in Eq. (25) for $j=\frac{3}{2}$ and in Eq. (26) for $j=\frac{1}{2}$, and $\mathcal{P}^A$ is defined by

$$\mathcal{P}^A([p_{jN}^{-1}s_{1/2\Lambda}]_{J=1^-})=\frac{-2\sqrt{2}\mathrm{Im}[\mathcal{A}(0)^*\mathcal{A}(1)]}{|\mathcal{A}(0)|^2+2|\mathcal{A}(1)|^2} \, , \quad (30)$$

which is independent of j. Here $\mathcal{A}(m)$ is $\mathcal{A}(1m)$ of Eq. (22).

The physical origin of $\mathcal{P}^A$ lies in the meson absorption or, more precisely, difference of the net absorption between near-side and far-side passing mesons. In fact, Eq. (30) was already obtained in Ref. 11. Figure 1 shows the calculated $\mathcal{P}$ against θ_{lab}. ($\mathcal{P}^A$ shown is that for $^{12}_\Lambda$C, but it changes for $^{16}_\Lambda$O only slightly.) $\mathcal{P}^A$ is negative except at very small angles. This can be understood in terms of the fact that near-side going mesons, which transfer an angular momentum to the $-\hat{\mathbf{n}}$ direction, are less absorbed than the others, and consequently the component with $M<0$ is more populated than that with $M>0$. The

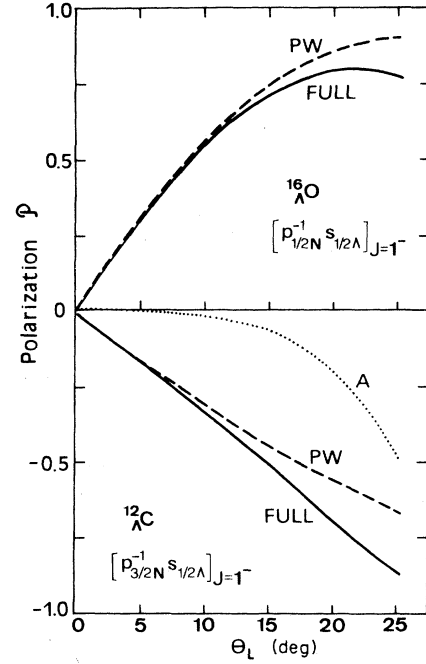
FIG. 1. Polarizations in the $[p_{3/2N}^{-1}s_{1/2\Lambda}]_{J=1^-}$ state of $^{12}_\Lambda$C and the $[p_{1/2N}^{-1}s_{1/2\Lambda}]_{J=1^-}$ state of $^{16}_\Lambda$O produced in the (π^+,K^+) reaction at $p_\pi=1.04$ GeV/c. The labels PW, A, and FULL denote, respectively, the plane-wave (no distortion) limit $\mathcal{P}^{\mathrm{PW}}$ of Eqs. (25) and (26), the absorption-originated (distorted wave) $\mathcal{P}^A$ of Eq. (30), and the full polarization of Eq. (29).

slightly positive values of $\mathcal{P}^A$ at small θ_{lab} are due to the fact that absorption of the incoming π^+ is stronger than that of the outgoing K^+.[11,12] The latter mechanism is also effective to make $\mathcal{P}^A$ small up to $\theta_{\mathrm{lab}}\sim15°$ through destructive interference in the near-side–far-side effect mentioned above. Anyway, the above two examples contrast the different origins which additively (destructively) work to make the polarization larger (smaller).

In obtaining the π^+ and K^+ distorted waves, we have employed the eikonal approximation together with the absorptive potentials given in terms of the empirical averaged π^+N and K^+N reaction cross sections. (For example, $\bar{\sigma}_{\pi^+N}=41$ mb and $\bar{\sigma}_{K^+N}=14$ mb at $p_\pi=1.04$

TABLE I. The calculated polarization $\mathcal{P}^{\mathrm{PW}}(\theta_{\mathrm{lab}})$ in the plane-wave (no distortion) limit for the (π^+,K^+) reaction at $p_\pi=1.04$ GeV/c. The four configurations $[N^{-1}\Lambda]_J$ are labeled by the corresponding equation numbers (25)–(28). $[(\mathrm{GeV}/c)^{-2}]$: (25)$=[p_{3/2}^{-1}s_{1/2}]_{1^-}$, (26)$=[p_{1/2}^{-1}s_{1/2}]_{1^-}$, (27)$=[p_{3/2}^{-1}p_{1/2}]_{2^+}$, (28)$=[p_{1/2}^{-1}p_{3/2}]_{2^+}$.

θ_{lab}	$|f|^2$	$|g|^2$	$\mathrm{Im}[fg^*]$	$\mathcal{P}_\Lambda^{\mathrm{elem}}$	(25)	(26)	(27)	(28)
0°	1.063	0	0	0	0	0	0	0
5°	1.028	0.033	0.169	0.31	−0.16	0.31	−0.23	0.23
10°	0.932	0.116	0.301	0.57	−0.31	0.57	−0.44	0.44
15°	0.794	0.214	0.378	0.75	−0.45	0.75	−0.60	0.60
20°	0.640	0.299	0.402	0.86	−0.56	0.86	−0.70	0.70
25°	0.493	0.352	0.386	0.91	−0.66	0.91	−0.77	0.77
30°	0.370	0.365	0.344	0.93	−0.75	0.93	−0.80	0.80

GeV/c.) The Λ and nucleon single-particle wave functions have been obtained by solving Skyrme Hartree-Fock (HF) equation with SIII NN (Ref. 14) and Rayet No. 13 ΛN (Ref. 15) interactions.

The calculated cross sections and polarizations are displayed in Fig. 2 for ^{12}C $(\pi^+, K^+)^{12}_\Lambda$C and in Fig. 3 for ^{28}Si$(\pi^+, K^+)^{28}_\Lambda$Si, where only configurations with the least bound neutron hole are shown.

Concerning $^{12}_\Lambda$C of Fig. 2, the unnatural parity states $(2^-, 3^+)$ grow up to ~ 1 μb/sr at $\theta_{\text{lab}} = 10°$–$15°$, where the natural parity states $(1^-, 2^+)$ already fall down to around 5 μb/sr. This non-negligible appearance of the unnatural parity states reflects the importance and magnitude of the spin-flip amplitude g relative to the spin-nonflip amplitude f at momentum $p_\pi = 1.04$ GeV/c. Note that the obtained cross sections reasonably agree with the experiment[2,4] which shows two peaks corresponding to the $[p^{-1}_{3/2N}s_{1/2\Lambda}]$ and $[p^{-1}_{3/2N}p_\Lambda]$ configurations. The polarizations of the $[p^{-1}_{3/2N}s_{1/2\Lambda}]_{J=1^-}$ and $[p^{-1}_{3/2N}p_{1/2\Lambda}]_{J=2^+_2}$ states are negative and as large as 50% at $\theta_{\text{lab}} = 10°$–$15°$ where the cross sections are still appreciable. The polarizations of the unnatural parity states are generally very small.

In Fig. 3, only natural parity states of $^{28}_\Lambda$Si are shown, divided into three blocks corresponding to three major Λ shells (actually three observed peaks[4]). Again very large polarizations are predicted. The $[d^{-1}_{5/2N}l_{j<\Lambda}]_{J_{\text{max}}}$ states acquire both large cross section and large polarization. A
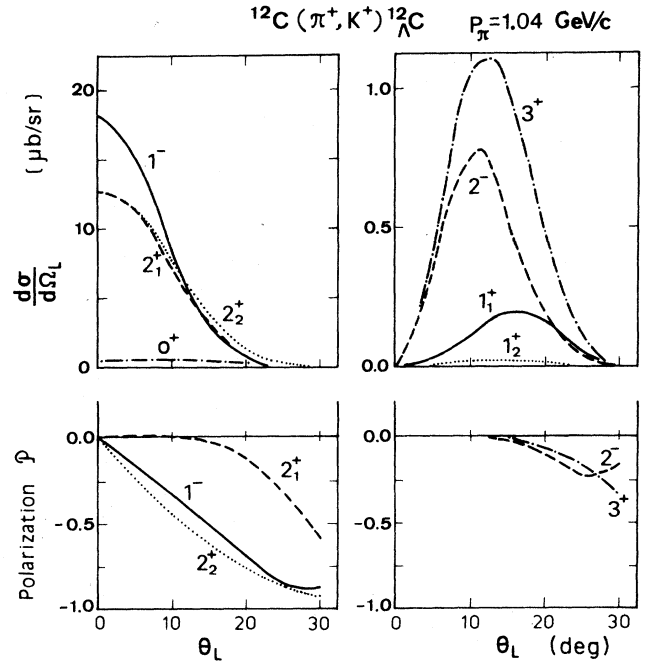

FIG. 2. The calculated cross sections and polarizations for the states of $^{12}_\Lambda$C, $[p^{-1}_{3/2N}s_{1/2\Lambda}]_{J=1^-2^-}$, $[p^{-1}_{3/2N}p_{3/2\Lambda}]_{J=0^+1^+_12^+_13^+}$, and $[p^{-1}_{3/2N}p_{1/2\Lambda}]_{J=1^+_22^+_2}$, produced in the (π^+, K^+) reaction at $p_\pi = 1.04$ GeV/c.

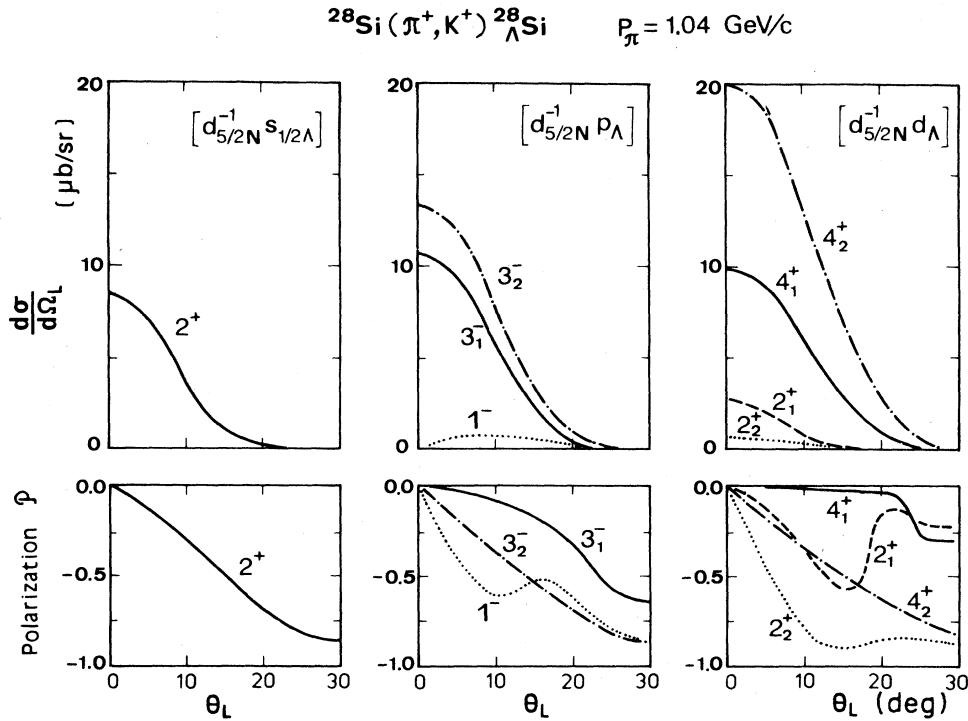

FIG. 3. The calculated cross sections and polarizations for the natural parity states of $^{28}_\Lambda$Si with a $(d_{5/2})$ neutron hole and a $(s_{1/2}, p_{3/2,1/2}, d_{5/2,3/2})$ Λ particle produced in the (π^+, K^+) reaction at $p_\pi = 1.04$ GeV/c. The J_1 and J_2 stand for $j_{>,\Lambda}$ and $j_{<,\Lambda}$, respectively.

nice feature is that polarizations of the states belonging to the same block are all of the same sign. This keeps polarization significant, even when those states cannot be separated in energy as is the case with the present experimental resolution.

Among unnatural parity states, the $[d_{5/2N}^{-1}p_{3/2\Lambda}]_{J=4^-}$ and $[d_{5/2N}^{-1}d_{5/2\Lambda}]_{J=5^+}$ states are the only two that attain the cross sections as large as ~ 1 μb/sr at $\theta_{lab}=10^\circ$–15°, while their polarizations are very small (just less than 2%).

Figure 4 displays another example: $^{56}_\Lambda$Fe, where the $[f_{7/2N}^{-1}l_{j<\Lambda}]_J$ and $[f_{7/2N}^{-1}l_{j>\Lambda}]_J$ states are grouped into the left and right halves, respectively, and only those with natural parity J_{max} are shown. Comparing the left- and right-hand figures, we see a clear difference in the behavior of $d\sigma/d\Omega_{lab}$ and $\mathcal{P}$ of these two combinations. For a series of states with Λ in $s_{1/2}$, $p_{1/2}$, $d_{3/2}$, and $f_{5/2}$, the cross sections increase in this order, while the polarizations are all comparably large. On the other hand, another series of states with Λ in $p_{3/2}$, $d_{5/2}$, and $f_{7/2}$ shows nonuniform behavior. Here again the selectivity of the (π^+,K^+) reaction, which preferentially populates the former type of states, is compatible with production of significant polarization.

Figures 5 and 6 show the dependence of the cross section and polarization on the incident pion momentum p_π for the elementary process $\pi^+n\to\Lambda K^+$ and the $^{12}_\Lambda$C$([p_{3/2N}^{-1}s_{1/2\Lambda}]_{J=1^-})$ state production, respectively. There, a wide range of the momentum p_π is considered,

since the elementary cross section, which has a prominent peak at $p_\pi=1.04$ GeV/c, starts to rise again at $p_\pi\sim1.8$ GeV/c, as seen in Fig. 5.

By comparing the upper halves of Figs. 5 and 6, one can see that the hypernuclear production cross sections at very forward angles ($\theta_{lab}\sim0^\circ$) are relatively enhanced with increasing incident momentum p_π. [The $\theta_{lab}=0^\circ$ cross-section ratio

$$\frac{d\sigma}{d\Omega}(p_\pi=1.04\text{ GeV}/c)\Big/\frac{d\sigma}{d\Omega}(p_\pi=2.4\text{ GeV}/c)$$

is ~1.5 in the elementary process, while ~0.5 in the hypernuclear production.] This is due to smaller transfer momenta and therefore larger sticking probabilities with increasing p_π. On the other hand, the hypernuclear production cross section at higher p_π drops very fast with the angle θ_{lab}, because large momenta even at small scattering angles yield sizable transfer momenta.

Suppose more than 50% polarization is needed, one has to go, with $p_\pi<1.3$ GeV/c beams, up to $\theta_{lab}\sim15^\circ$, where the cross section is less than 3 μb/sr. If beams with $p_\pi=1.3$–1.6 GeV/c are used, $\theta_{lab}=10^\circ$ is enough for 50% polarization but again with the cross section less than 3 μb/sr. A choice of $p_\pi=1.6$–1.9 GeV/c and $\theta_{lab}=5^\circ$ gives 5–9 μb/sr for cross section and 50–70% for polarization. Of course, the actual choice of the p_π and θ_{lab} depends severely on the instrumental limitation.
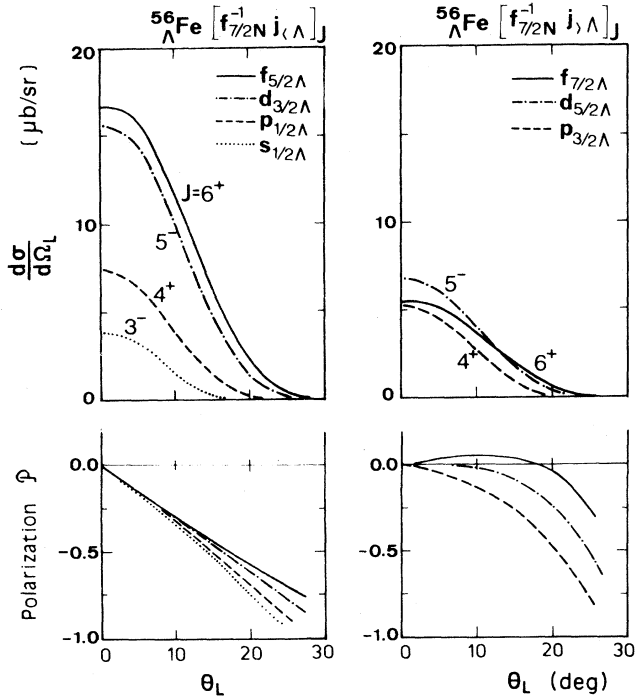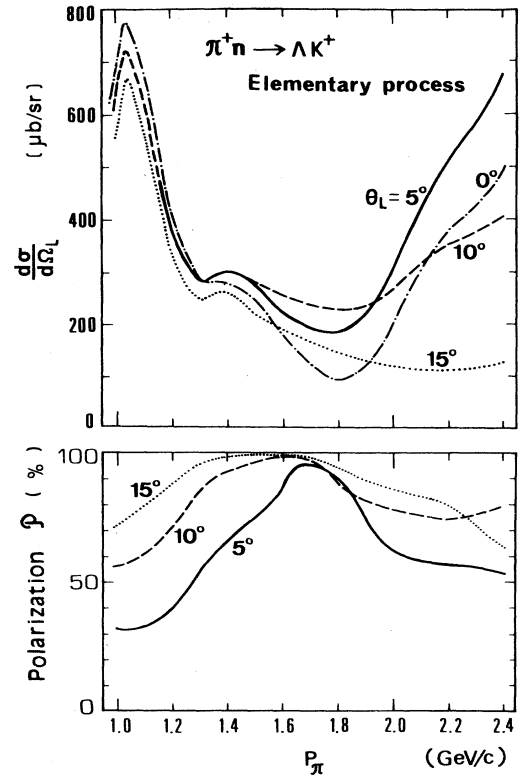

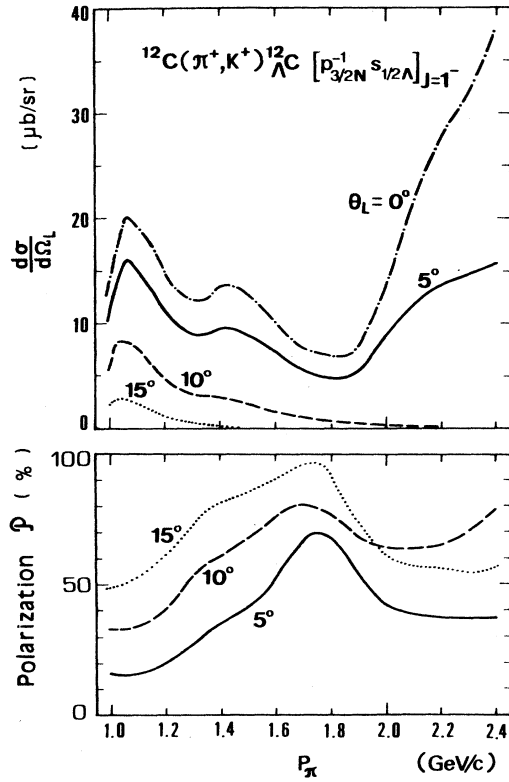FIG. 4. The calculated cross sections and polarizations for the natural-parity high-spin states of $^{56}_\Lambda$Fe with a $(f_{7/2})$ neutron hole. $p_\pi=1.04$ GeV/c.

FIG. 5. The incident-pion-momentum dependence of the cross sections and polarizations at $\theta_{lab}=0^\circ$, 5°, 10°, and 15° for the elementary $\pi^+n\to\Lambda K^+$ process.

FIG. 6. The incident-pion-momentum dependence of the production cross sections and polarizations at $\theta_{lab}=0°$, $5°$, $10°$, and $15°$ for the ground state of $^{12}_\Lambda C$.

Nonetheless, the results displayed in Fig. 6 should be useful for considering what is the optimal choice in the realistic situation.

IV. CONCLUDING REMARKS

The cross sections and polarizations for the hypernuclear states produced in the (π^+, K^+) reaction have been described in terms of the spin-nonflip f and spin-flip g amplitudes, the π^+ and K^+ distorted waves, and the parent nuclear and daughter hypernuclear wave functions. No previous works have treated the g amplitude explicitly even in evaluating the cross section only. Tabulation of the amplitudes in a convenient form for practical use[13] has made the present calculation possible.

Of the two different origins of polarization, f-g interference (intrinsic spin orientation) and meson absorption (orbital angular momentum orientation), the former has been found to prevail at $\theta_{lab}=10°-15°$ where both cross section and polarization are significantly large for particular hypernuclear states. This reflects, of course, very large polarization in the elementary $\pi N \to K \Lambda$ process. Recall that a selectivity characteristic to the (π^+, K^+) reaction is the strongest population (cross section) of the $[j_{>N}^{}j_{<\Lambda}]_{J_{max}}$ and $[j_{<N}^{-1}j_{>\Lambda}]_{J_{max}}$ configurations.[3] The examples given in Sec. III show that the same configurations also acquire large polarization, which is important for their measurability.

The polarized hypernucleus is especially useful, when combined with coincidence measurement of the secondary decay particles. Asymmetry of weak-decay pions provides important information on hypernuclear structure and also on pion distortion in nuclear deep interior.[16] The angular pattern of protons from nonmesonic decay of polarized hypernucleus sensitively reflects the mechanism of this two-body weak interaction in nuclear medium.[9,11] The polarization may be also applied to measure the magnetic moment of Λ hyperon in hypernuclei.[9] Such experiments are in fact under consideration at the National Laboratory for High Energy Physics (KEK) in anticipation of improvements of the beam intensity and spectrometer systems. The present study gives theoretical basis for attempting such novel experiments.

APPENDIX: EXPRESSIONS OF $\rho(if; M_f)$

The three $\rho(if; M_f)$ in Eq. (13) are, respectively, expressed as

$$\rho^{ff}(if; M_f) = \frac{4\pi}{[J_i]} \sum_{k_1 k_2} \sum_K \sqrt{[k_2][k_2]}(-)^{J_i - M_f} i^{k_1 - k_2} W(k_1 k_2 J_f J_f; K J_i)(J_f M_f J_f - M_f | K 0)$$

$$\times \sum_{m_1 m_2} (-)^{k_1 + k_2 - K} (-)^{m_2} (k_1 m_1 k_2 - m_2 | K q)$$

$$\times i^{|q|} d(K, q) \langle J_f || \tilde{j}_{k_2 m_2} Y_{k_2} || J_i \rangle_{S_1}^* \langle J_f || \tilde{j}_{k_1 m_1} Y_{k_1} || J_i \rangle_{S_1} , \qquad (A1)$$

$$\rho^{gg}(if;M_f) = \frac{4\pi}{[J_i]} \sum_{k_1 k_2} \sum_{K_1 K_2} \sqrt{[k_1][k_2][K_1][K_2]}(-)^{k_1+k_2+K_1+K_2+1}(-)^{J_i-M_f} i^{k_1-k_2}$$

$$\times \sum_{\kappa p p'} W(K_1 K_2 J_f J_f; \kappa J_i)(J_f M_f J_f - M_f | \kappa 0) W(K_1 K_2 k_1 k_2; p1)$$

$$\times \sum_m (K_1 - m K_2 m | \kappa 0)(K_1 m K_2 - m | p0)(k_1 - m k_2 m | p0)(k_1 m k_2 - m | p'0)$$

$$\times \sum_{m_1 m_2} (-)^{m_2}(k_1 m_1 k_2 - m_2 | p'q) i^{|q|} d(p',q) \langle J_f || \tilde{j}_{k_2 m_2}[Y_{k_2} \times \sigma]_{K_2} || J_i \rangle^*_{S_1}$$

$$\times \langle J_f || \tilde{j}_{k_1 m_1}[Y_{k_1} \times \sigma]_{K_1} || J_i \rangle_{S_1} , \tag{A2}$$

$$\rho^{fg}(if;M_f) = \frac{4\pi}{[J_i]} \sum_{k_1 k_2} \sum_{K} \sqrt{[k_1][k_2][K]}(-)^{k_1+k_2}(-)^{J_i-M_f} i^{k_1-k_2}$$

$$\times \sum_{\kappa p} \sqrt{[p]} W(k_1 K J_f J_f; \kappa J_i)(J_f M_f J_f - M_f | \kappa 0) W(k_1 k_2 \kappa 1; pK)(-)^p(p010 | \kappa 0)$$

$$\times \sum_{m_1 m_2} (-)^{m_2}(k_1 m_1 k_2 - m_2 | pq) i^{|q|} d(p,q)$$

$$\times \langle J_f || \tilde{j}_{k_2 m_2}[Y_{k_2} \times \sigma]_K || J_i \rangle^*_{S_1} \langle J_f || \tilde{j}_{k_1 m_1} Y_{k_1} || J_i \rangle_{S_1} , \tag{A3}$$

where

$$d(p,q) = \begin{cases} (-)^{(p+|q|)/2} \left[\dfrac{(p-|q|)!}{(p+|q|)!} \right]^{1/2} \dfrac{1}{2^p} \dfrac{(p+|q|)!}{\left[\dfrac{p-|q|}{2}\right]! \left[\dfrac{p+|q|}{2}\right]!} & \text{for } p+q = \text{even}, \\ 0 \quad \text{for } p+q = \text{odd}. \end{cases} \tag{A4}$$

Symbolic expressions of matrix elements $\langle \, || \, || \, \rangle$ are self-explanatory.

*Also at Institute for Nuclear Study, University of Tokyo, Tanashi, Tokyo 188, Japan.

[1]C. B. Dover, L. Ludeking, and G. Walker, Phys. Rev. C 22, 2073 (1980).

[2]C. Milner et al., Phys. Rev. Lett. 54, 1237 (1985).

[3]H. Bandō and T. Motoba, Prog. Theor. Phys. 76, 1321 (1986).

[4]R. E. Chrien, Nucl. Phys. A478, 705c (1988).

[5]T. Motoba, H. Bandō, R. Wünsch, and J. Žofka, Osaka Electro-Communication University Report OECU-1987-12 (1987); Phys. Rev. C 38, 1322 (1988).

[6]W. Brückner et al., Phys. Lett. 55B, 107 (1975); 62B, 481 (1976); 79B, 157 (1978); R. Bertini et al., Nucl. Phys. A360, 315 (1982); B. Povh, Rep. Prog. Phys. 39, 824 (1976); Annu. Rev. Nucl. Part. Sci. 28, 1 (1978).

[7]M. Bedjidian et al., Phys. Lett. 94B, 480 (1980); M. May et al., Phys. Rev. Lett. 51, 2085 (1983).

[8]R. Grace et al., Phys. Rev. Lett. 55, 1055 (1985); P. D. Barnes and J. J. Szymanski, Proceedings of the INS International Symposium on Hypernuclear Physics, Tokyo, 1986, edited by H. Bandō, O. Hashimoto, and K. Ogawa (Institute for Nu-

clear Study, University of Tokyo, Tokyo, 1986), p. 136; P. D. Barnes, Nucl. Phys. A478, 127c (1988).

[9]T. Fukuda, H. Ejiri, T. Shibata, H. Bandō, and T. Motoba, Proceedings of the INS International Symposium on Hypernuclear Physics, Tokyo, 1986 (Institute for Nuclear Study, University of Tokyo, Tokyo, 1986), p. 170.

[10]R. D. Baker, et al., Nucl. Phys. B126, 365 (1977); B141, 29 (1978); D. H. Saxon et al., ibid. B162, 522 (1980); K. W. Bell et al., ibid. B222, 389 (1983).

[11]H. Bandō, Genshikaku Kenkyu 31, 99 (1986).

[12]H. Ejiri, T. Fukuda, T. Shibata, H. Bandō, and K.-I. Kubo, Phys. Rev. C 36, 1435 (1987).

[13]M. Sotona and J. Žofka, Institute for Nuclear Study, University of Tokyo Report INS-Rep-683, 1988.

[14]D. Vautherin and D. M. Brink, Phys. Rev. C 5, 626 (1972).

[15]M. Rayet, Nucl. Phys. A367, 381 (1981).

[16]T. Motoba, K. Itonaga, and H. Bandō, Osaka University Applied Mathematics Report OUAM-88-7-2, 1988; Nucl. Phys. A (to be published).